Observation of Photon Droplets and Their Dynamics

Kali E. Wilson,[1,*] Niclas Westerberg,[1] Manuel Valiente,[1] Callum W. Duncan,[1] Ewan M. Wright,[2,1] Patrik Öhberg,[1] and Daniele Faccio[1,3,†]

[1]*Institute of Photonics and Quantum Sciences, Heriot-Watt University, Edinburgh EH14 4AS, United Kingdom*
[2]*College of Optical Sciences, University of Arizona, Tucson, Arizona 85721, USA*
[3]*School of Physics and Astronomy, University of Glasgow, Glasgow G12 8QQ, United Kingdom*

(Received 8 February 2018; published 27 September 2018)

We present experimental evidence of photon droplets in an attractive (focusing) nonlocal nonlinear medium. Photon droplets are self-bound, finite-sized states of light that are robust to size and shape perturbations due to a balance of competing attractive and repulsive forces. It has recently been shown theoretically, via a multipole expansion of the nonlocal nonlinearity, that the self-bound state arises due to competition between the *s*-wave and *d*-wave nonlinear terms, together with diffraction. The theoretical photon droplet framework encompasses both a solitonlike stationary ground state and the nonsolitonlike dynamics that ensue when the system is displaced from equilibrium, i.e., driven into an excited state. We present numerics and experiments supporting the existence of these photon droplet states and measurements of the dynamical evolution of the photon droplet orbital angular momentum.

DOI: 10.1103/PhysRevLett.121.133903

Vortex beams in local nonlinear media experience symmetry-breaking azimuthal instabilities [1–4]. Nonlocal nonlinearities can stabilize such beams [5,6]; solitary-wave behavior for both Laguerre-Gauss (LG) [7] and Hermite-Gauss (HG) modes [8] has been demonstrated experimentally with a laser beam propagating through a thermal nonlinear medium. The theoretical treatment for such behavior stems from the Snyder-Mitchell (SM) model for accessible solitons [9], where the effective potential due to the attractive (focusing) nonlocal nonlinearity is approximated by a parabolic function, with a local minimum at $r = 0$ [10–12]. For sufficiently high nonlocality, a vortex beam with orbital angular momentum (OAM) constitutes a stable soliton solution of the nonlocal nonlinear Schrödinger equation (nonlocal NLSE) [13]. However, the nonlocality must be much greater than the beam size in order to allow the effective nonlinear potential to remain parabolic regardless of the shape of the input beam [14,15]. The dynamics of structured beams, such as dipole solitons [16,17], azimuthons [10,18], and higher-order HG beams [19], have been explored either within the SM potential or through a purely numerical treatment of the nonlocal nonlinearity.

Recent theoretical work has introduced the concept of photon droplets, or droplets of light, defining them as "self-bound, finite-sized objects that are stable against perturbations in size, shape, and density due to a competition of attractive and repulsive forces" [14]. We consider a soliton to be a beam whose transverse spatial profile does not change under propagation. The definition of a photon droplet does not require stationarity; however, if a droplet is initiated in the ground state, then its stationary behavior will coincide with the solitons described above. Liquid light states have also been proposed, arising from the balance between higher-order, cubic-quintic nonlinearities [20–22] that are distinct from the photon droplets. In the photon droplet framework, a beam of light propagating in a nonlocal nonlinear medium is treated as a many-body system where the photon-photon interaction is mediated by the nonlinearity Δn. A multipole expansion of Δn allows the calculation of a pseudoenergy landscape for the many-body photon state [14], as a function of the state's physical size and net OAM. The expansion reveals competition between an *s*-wave nonlinear term favoring a stable vortex ring [13] and a *d*-wave nonlinear term favoring a two-lobed structure [see Fig. 1(b)]. This competition together with kinetic energy (diffraction) results in a robust, *p*-wave-symmetric self-bound state, with a lower

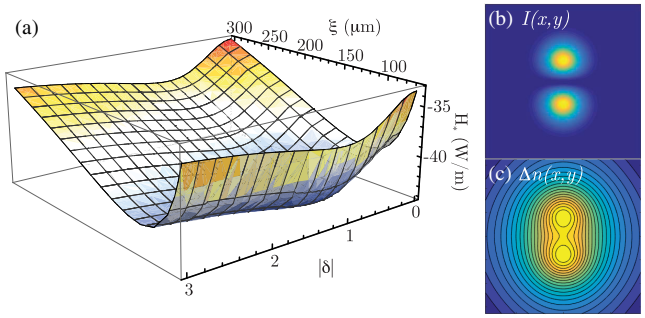

FIG. 1. (a) Pseudoenergy landscape $H_*(\delta, \xi)$ for $P_0 = 0.8$ W and $E_0(r) \propto re^{-r^2/\xi_0^2}$. (b),(c) 320 μm × 320 μm square images showing the transverse intensity profile $I(x, y)$ and nonlinear potential $\Delta n(x, y)$, respectively, for the ground state. The minimum pseudoenergy occurs for $|\delta| = 1$ and $\xi \sim 100$ μm, and there is an instability at $H_*(\delta = 0)$ in contrast to the SM model.

pseudoenergy than that of the azimuthally symmetric SM vortex soliton [14]. The energy-landscape description enabled by the multipole expansion of Δn encompasses both a stationary lowest-energy state, with p-wave symmetry and zero net OAM, and the dynamics of a broader class of excited states including the rotating dipole solitons and azimuthons discussed above. Photon droplets extend beyond these concepts, attain liquidlike properties, and exhibit a liquid-to-gas transition concurrent with the emergence of sound waves as low-energy excitations. Furthermore, their pseudoenergy per unit power, analogous to the energy per particle [23], has the same form as the equation of state (EOS) for droplets of one-dimensional liquid helium [14,24] and shares similarities with the EOS for droplets found in Bose-Einstein condensates (BECs) [25–29]. While inherently quantum, BEC droplets are often described by a classical Gross-Pitaevskii equation, where an effective classical potential accounts for the quantum-fluctuation stabilization term [26].

In this Letter, we provide the first experimental evidence of photon droplets and study their evolution. We focus attention on the out-of-equilibrium dynamics characterized by evolution of the droplet angular momentum. Experimental OAM-mode decomposition measurements show that the net OAM of the photon droplet varies as it propagates. The droplet and higher-order OAM excitations exchange OAM back and forth as the photon droplet explores its pseudoenergy landscape in a manner reminiscent of the two-way energy exchange between a hot spot and the photon bath in optical filamentation [30].

In our experiment, a beam with a p-wave symmetric intensity profile propagates through an attractive (focusing) nonlocal nonlinear medium, in this case lead-doped glass (SF6) with a thermal nonlinearity characterized by $\beta = -dn/dT = 14 \times 10^{-6}\ \mathrm{K}^{-1}$, a heat capacity of $\kappa = 0.7\ \mathrm{W\,m^{-1}\,K^{-1}}$, linear absorption $\alpha = 0.01\ \mathrm{cm}^{-1}$, and a background index of refraction $n_0 = 1.8$ [31]. The propagation of the electric field $E(\mathbf{r}, z)$ through this medium is described by the NLSE

$$i\frac{\partial E}{\partial z} = -\frac{1}{2k_0}\nabla^2 E - \frac{k_0}{n_0}\Delta n E - \frac{i\alpha}{2}E \equiv \mathcal{H}_* E. \tag{1}$$

Here $k_0 = 2\pi n_0/\lambda$ is the wave number in the medium and, for light of vacuum wavelength λ, ∇^2 is the two-dimensional Laplacian for the transverse plane $\mathbf{r} = (x, y)$. In analogy to BECs, $\mathcal{H}_*$ is the pseudoenergy density, E plays the role of the many-body wave function, and the propagation direction z maps to time [32]. The nonlocal nonlinearity $\Delta n = \gamma \int d^2r' R(\mathbf{r} - \mathbf{r}')|E(\mathbf{r}', z)|^2$ is well described by the real space response function $R(\mathbf{r}) = K_0(|\mathbf{r}|/\sigma)/2\pi\sigma^2$. Here $\gamma = \alpha\beta\sigma^2/\kappa = 1.25 \times 10^{-6}\ \mathrm{cm^2\,W^{-1}}$ gives the nonlinear coefficient characterized by the physical system parameters, and K_0 is the zeroth-order modified Bessel function of the second kind. The nonlocal length $\sigma = D/2 = 2.5$ mm is fixed to half the smallest dimension of the material, which is a valid assumption for a rectangular geometry in the steady-state regime with $\Delta T = 0$ at the boundary [31,33]. Over the extent of the beam, the measured response function is to a good approximation radially symmetric. We evaluate the pseudoenergy functional [14]

$$H_* = \int d^2r' E^*(\mathbf{r}', z)\mathcal{H}_*(\mathbf{r}', z)E(\mathbf{r}', z), \tag{2}$$

where $\mathcal{H}_*$ is defined in Eq. (1), and the corresponding Lagrangian density is $\mathcal{L} = E^*(i\partial_z - \mathcal{H}_*)E$. To evaluate H_* analytically, we choose the ansatz

$$E(\mathbf{r}, 0) \propto re^{-r^2/\xi_0^2}[e^{i\phi} + \delta_0 e^{-i\phi}] \tag{3}$$

for the input beam, where ϕ is the azimuthal angle in cylindrical coordinates, $\xi_0 = \xi(z = 0)$ is the $1/e^2$-intensity beam radius, and $\delta_0 = \delta(z = 0)$ gives the ratio of OAM $\ell = -1$ to $\ell = +1$ [34]. We perform a multipole expansion of the nonlocal nonlinearity

$$\Delta n \approx \gamma\left[P - d_\nu \partial^\nu_{\mathbf{r}} + \frac{1}{2}Q_{\nu,\mu}\partial^\nu_{\mathbf{r}}\partial^\mu_{\mathbf{r}}\right]R(\mathbf{r}), \tag{4}$$

where P is the power, $d_\nu = \langle x_\nu \rangle$ is the Cartesian ν component of the dipole moment, and $Q_{\nu,\mu} = \langle x_\nu x_\mu \rangle$ is the corresponding element of the quadrupole moment tensor. We refer to this expansion of the nonlocal nonlinearity as the long wavelength approximation (LWA), which is valid for a tightly bound scenario ($\sigma \gg \xi$) [14]. For an input beam of the form of Eq. (3), the dipole moment cancels, leaving a competition between the linear s-wave and quadrupole d-wave terms resulting in the pseudoenergy landscape $H_*(\delta, \xi)$ shown in Fig. 1(a). In analogy with BEC droplets [25,26], the bound state depends on the number of particles in the system, which in this case is the beam power. As shown in Fig. 1, we find a clear minimum associated with $|\delta| = 1$, corresponding to a two-lobed photon droplet with zero OAM, and a power-dependent value of $\xi = \xi_{\min}$. At higher powers, the depth of the pseudoenergy well increases, and $\xi_{\min}$ decreases [14]. Figures 1(b) and 1(c) show the transverse intensity profile $I(x, y)$ and corresponding nonlinear potential $\Delta n(x, y)$ for the lowest-energy photon droplet.

We solve Eq. (1) numerically [31], using the k-space response function $\hat{R}(k_x, k_y) = 1/[1 + \sigma^2(k_x^2 + k_y^2)]$ [33] to account for the nonlocality associated with the nonlinearity, $\Delta\hat{n}(k_x, k_y) = \gamma\hat{R}(k_x, k_y)\hat{I}(k_x, k_y)$, where $\hat{I}(k_x, k_y)$ is the Fourier transform of $I(x, y)$. We map the photon droplet dynamics to the pseudoenergy landscape by calculating $|\delta| = |c_-|/|c_+|$ and the photon droplet radius $\langle r \rangle = \int r|E|^2 r dr d\phi / \int |E|^2 r dr d\phi \propto \xi$ as the beam propagates. Here c_+ (c_-) is the amplitude of the electric field associated with OAM $\ell = +1$ ($\ell = -1$) calculated by decomposing

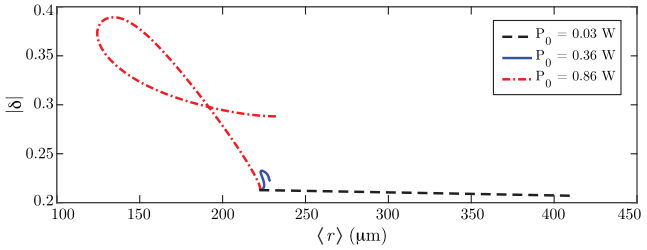

FIG. 2. Photon droplet dynamics from numerics. Plot of $|\delta|$ versus $\langle r \rangle \propto \xi$ over 80 cm of propagation for $|\delta_0| = 0.2$, $\xi_0 = 210\ \mu$m ($\langle r \rangle_0 = 220\ \mu$m), and varying input beam powers P_0. See Supplemental Material [35] for details of the spatial evolution.

the transverse electric field from the numerics onto an orthonormal basis of LG beams.

Figure 2 shows plots of $|\delta|$ versus $\langle r \rangle$ for varying input power over 80 cm of propagation, for initial conditions $|\delta_0| = 0.2$ and $\xi_0 = 210\ \mu$m ($\langle r \rangle_0 = 220\ \mu$m). These plots show how the relevant physical parameters evolve as the photon droplet explores its pseudoenergy landscape $H_*(\delta, \xi \sim \langle r \rangle)$. For low particle numbers (dashed black line, $P_0 = 0.03$ W), we observe near-constant $|\delta|$ as the radius increases, corresponding to linear diffraction in the absence of a bound-state or pseudoenergy well: The analogous particle number is less than what is required for a bound state to form, a common feature of droplets. For intermediate particle numbers (solid blue line, $P_0 = 0.36$ W), we observe small variations in both $|\delta|$ and $\langle r \rangle$, consistent with the low nonlinearity and correspondingly shallow pseudoenergy well at this power. Here we have nearly matched the ground state radius $\xi_{\min} \sim 200\ \mu$m for $P_0 = 0.36$ W, but $|\delta_0| = 0.2$ implies the photon droplet is displaced from equilibrium. Changes in $|\delta|$ must correspond to excitations of higher-order OAM modes such that the total OAM of the system remains constant. At $P_0 = 0.36$ W, there is a shallow pseudoenergy well [approximately 1/10 the depth of the one shown in Fig. 1(a)], but, given that the OAM of the system must be conserved, there is no path for the droplet to decay to lower energy; OAM-conserving excitations are too costly. For large particle numbers (dashed red line, $P_0 = 0.86$ W), we observe focusing in $\langle r \rangle$ and simultaneous variation in $|\delta|$. The energy landscape is now steeper [see Fig. 1(a)], so high-energy excitations corresponding to higher-order OAM modes may be energetically allowed.

Figure 3 shows our experimental setup. We use a 532-nm laser with a Gaussian transverse beam profile. Lenses $L1$ and $L2$ expand the beam to a $1/e^2$-intensity beam radius of ~3 mm. We use a spatial light modulator (SLM) to create a diffraction grating with variable combinations of OAM $\ell = +1$ and $\ell = -1$. The SLM weakly focuses ($f \sim 2$ m) the first diffracted order onto the entrance facet $P0$ of a set of glass slabs (SF6). The power in the beam is varied from $P_0 = 30$ mW corresponding to linear propagation to

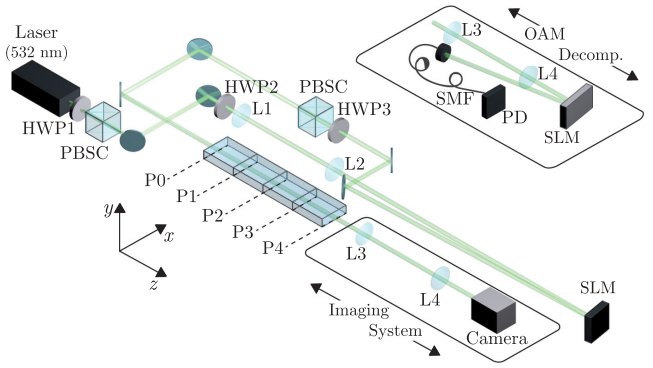

FIG. 3. Experimental setup. Lenses $L1$ and $L2$ expand the 532-nm laser beam. An SLM creates a diffraction grating with variable combinations of OAM $\ell = +1$ and $\ell = -1$. The first-order diffraction is weakly focused ($f \sim 2$ m) onto the entrance facet ($P0$) of a set of four 10-cm × 4-cm × 0.5-cm glass slabs. HWP2 is used to vary the SLM diffraction efficiency. HWP3 and PBSC provide additional control of P_0. The beam intensity profile is imaged at the entrance facet $P0$ and at the exit facet of each glass plate $P1$–$P4$. The $M = 6$ imaging system is fixed with respect to the camera and translated as a single entity. The camera can be replaced with an SLM and single-mode fiber to perform an OAM decomposition.

$P_0 = 0.86$ W. This results in an initial state $E(r, z = 0)$ at $P0$ that is a good approximation of the ansatz of Eq. (3). The 40-cm-long glass sample is composed of four slabs, each 10 cm × 4 cm × 0.5 cm, placed one after the other. We monitor the beam evolution at 10 cm intervals by imaging the output at successive planes, $P0$–$P4$, as indicated in Fig. 3 [36]. The camera and optics for the imaging system with magnification $M = 6$ are shifted as a unit to image each plane in succession, allowing us to follow the evolution of the photon droplet in "time" for a fixed input power.

An interesting question arises in relation to whether an excited state with nonzero OAM ($|\delta| \neq 1$) can explore the full energy landscape (varying both $|\delta|$ and ξ). Evolution of $|\delta|$ implies a change in the net angular momentum of the photon droplet. To reconcile this, the photon droplet is expected to excite higher-order OAM modes as it relaxes towards $|\delta| = 1$. As the system is (mostly) closed, however, such excitations cannot escape, and we expect that higher-order OAM excitations are reabsorbed by the droplet at a later "time," leading to beating dynamics in both ξ and $|\delta|$. To study this, we choose an initial state with $|\delta_0| = 0.7$ and $\xi_0 = 160\ \mu$m, shown in Fig. 4. Figure 4(a) shows experimental evolution of a beam with $P_0 = 0.03$ W to provide a linear propagation reference. Figures 4(b) and 4(c) show the experimental and corresponding numerical profiles, respectively, for $P_0 = 0.86$ W. Figure 4(d) shows plots of droplet rotation angle θ as a function of z calculated from numerics using the input parameters of Figs. 4(a) and 4(b).

We demonstrate the dynamical evolution of the photon droplet by measuring the OAM spectrum of the beam at

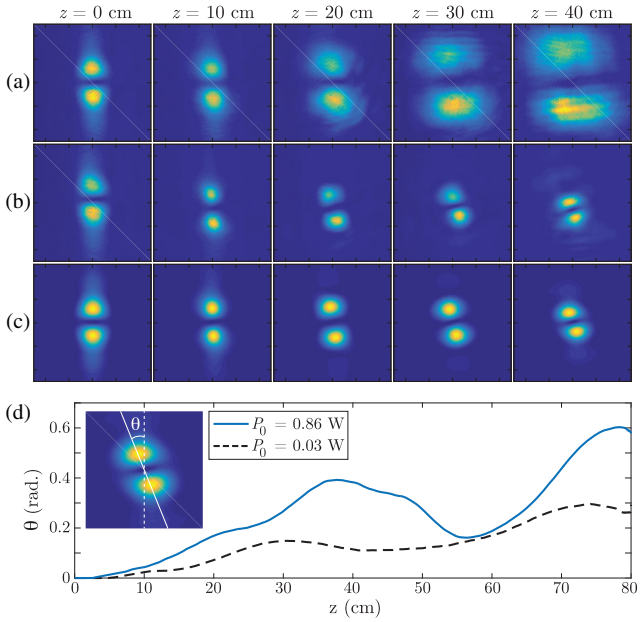

FIG. 4. 1-mm × 1-mm square images of the intensity profile for input conditions $|\delta_0| = 0.7$ and $\xi_0 = 160\ \mu$m. (a) Experiment: Effectively linear propagation for reference $P_0 = 0.03$ W. (b) Experiment: Photon droplet propagation for $P_0 = 0.86$ W. (c) Numerics: Propagation for $P_0 = 0.86$ W. (d) Numerics: Plots of rotation angle θ versus z.

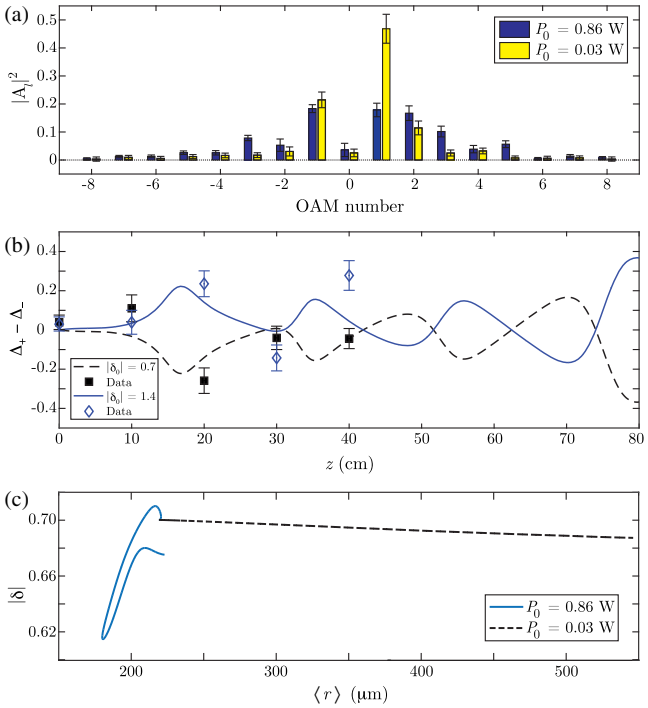

FIG. 5. Photon droplet dynamics with $\xi_0 = 160\ \mu$m. (a) Representative experimental OAM spectrum, after 20 cm of propagation for $|\delta_0| = 0.7$. (b) Plot of $\Delta_+ - \Delta_-$ versus z, where $\Delta_\pm = |A_{\mathrm{HP},\pm}|^2 - |A_{\mathrm{LP},\pm}|^2$. HP (LP) denotes $P_0 = 0.86$ W ($P_0 = 0.03$ W). Dashed black line: Numerics for $|\delta_0| = 0.7$. Solid blue line: Numerics for $|\delta_0| = 1.4$. Black squares: Experiment with $|\delta_0| = 0.7$. Blue diamonds: Experiment with $|\delta_0| = 1.4$. (c) Plot of $|\delta|$ versus $\langle r \rangle$ from numerics with $|\delta_0| = 0.7$.

planes $P0$–$P4$. We replace the camera with a second SLM (see Fig. 3, inset) and perform an OAM mode decomposition [37–39]. We display a series of forked diffraction gratings onto the SLM associated with a given OAM number ℓ_G, couple the first diffraction order into a single-mode fiber, and measure the intensity of the coupled light with a photodiode. Only the component of the field without an OAM ($\ell = 0$) efficiently couples into the single-mode fiber, such that for a diffraction grating with OAM ℓ_G, the photodiode measures $|A_{-\ell_G}|^2$, the amplitude of the component of $E(r, z)$ with OAM $\ell = -\ell_G$. We also calculate $|A_\ell|^2 = |\int E e^{-i\ell\phi} r dr d\phi|^2$ from the corresponding numerical simulation and normalize to $\sum |A_\ell|^2 = 1$.

Figure 5(a) shows a representative experimental OAM spectrum $|A_\ell|^2$ versus OAM number ℓ after 20 cm of propagation, showing that the photon droplet loses OAM by coupling to higher-order OAM modes. We quantify the net OAM in the photon droplet by calculating $\Delta_+ - \Delta_-$, where $\Delta_\pm = |A_{\mathrm{HP},\pm}|^2 - |A_{\mathrm{LP},\pm}|^2$, + (−) denotes $\ell = +1$ ($\ell = -1$), HP denotes $P_0 = 0.86$ W, and LP denotes the linear reference with $P_0 = 0.03$ W. Calculating $\Delta_+ - \Delta_-$ accounts for the systematic error due to any small changes in alignment in the experimental OAM measurement. Figure 5(b) shows plots of $\Delta_+ - \Delta_-$ versus z for $|\delta_0| = 0.7$ (numerics, dashed black line; data, black squares) and $|\delta_0| = 1.4$ (numerics, solid blue line; data, open blue diamonds) [40]. As seen in Fig. 5(b), $\Delta_+ - \Delta_-$ varies with z, a clear demonstration that the relative balance of $|A_+|^2$ and $|A_-|^2$ changes as the photon droplet evolves. The dynamical evolution of $|\delta|$ versus $\langle r \rangle$ calculated from the complementary numerics and plotted in Fig. 5(c) shows how the relevant physical parameters evolve as the photon droplet explores its pseudoenergy landscape.

In conclusion, we identify a robust self-bound photon droplet propagating in a nonlocal nonlinear medium. We show experimentally and numerically that a photon droplet displaced from equilibrium will exchange OAM back and forth with higher-order OAM modes as the photon droplet evolves in a manner reminiscent of the two-way energy exchange between a hot spot and the photon bath in optical filamentation [30]. The photon droplet description presented here provides a framework for exploring both a stationary solitonlike ground state and the dynamics associated with higher-energy excited states. These classical photon droplet states share a remarkable similarity to quantum droplets of dipolar BECs and 1D liquid helium and may give insight into the behavior of quantum [41] and classical [42] rotating droplets.

D. F. acknowledges financial support from the European Research Council under the European Union's Seventh Framework Program (FP/2007-2013)/ERC GA 306559,

the Engineering and Physical Sciences Research Council (EPSRC, United Kingdom, Grant No. EP/P006078/2). N. W. and C. W. D. acknowledge support from EPSRC CM-CDT Grant No. EP/L015110/1. M. V. and P. Ö. acknowledge support from EPSRC EP/M024636/1.

*kali.e.wilson@durham.ac.uk
†Daniele.Faccio@glasgow.ac.uk

[1] R. Y. Chiao, E. Garmire, and C. H. Townes, Phys. Rev. Lett. **13**, 479 (1964).
[2] A. S. Desyatnikov, Y. S. Kivshar, and L. Torner, *Progress in Optics*, edited by E. Wolf (Elsevier, New York, 2005), Vol. 47, pp. 291–391.
[3] V. Tikhonenko, J. Christou, and B. Luther-Daves, J. Opt. Soc. Am. B **12**, 2046 (1995).
[4] D. V. Petrov, L. Torner, J. Martorell, R. Vilaseca, J. P. Torres, and C. Cojocaru, Opt. Lett. **23**, 1444 (1998).
[5] A. S. Desyatnikov and Y. S. Kivshar, in *The Angular Momentum of Light*, edited by D. L. Andrews and M. Babiker (Cambridge University Press, Cambridge, England, 2012), Chap. 4, p. 71.
[6] D. Suter and T. Blasberg, Phys. Rev. A **48**, 4583 (1993).
[7] C. Rotschild, O. Cohen, O. Manela, M. Segev, and T. Carmon, Phys. Rev. Lett. **95**, 213904 (2005).
[8] C. Rotschild, M. Segev, Z. Xu, Y. V. Kartashov, L. Torner, and O. Cohen, Opt. Lett. **31**, 3312 (2006).
[9] A. W. Snyder and D. J. Mitchell, Science **276**, 1538 (1997).
[10] S. Lopez-Aguayo, A. S. Desyatnikov, Y. S. Kivshar, S. Skupin, W. Krolikowski, and O. Bang, Opt. Lett. **31**, 1100 (2006).
[11] D. Buccoliero, A. S. Desyatnikov, W. Krolikowski, and Y. S. Kivshar, Phys. Rev. Lett. **98**, 053901 (2007).
[12] D. Buccoliero, A. S. Desyatnikov, W. Krolikowski, and Y. S. Kivshar, Opt. Lett. **33**, 198 (2008).
[13] A. I. Yakimenko, Y. A. Zaliznyak, and Y. Kivshar, Phys. Rev. E **71**, 065603 (2005).
[14] N. Westerberg, K. E. Wilson, C. W. Duncan, D. Faccio, E. M. Wright, P. Öhberg, and M. Valiente, arXiv:1801.08539.
[15] M. S. Petrović, N. B. Aleksić, B. N. Aleksić, A. I. Strinić, and M. R. Belić, Phys. Rev. A **95**, 057801 (2017).
[16] M.-f. Shih, M. Segev, and G. Salamo, Phys. Rev. Lett. **78**, 2551 (1997).
[17] A. Fratalocchi, A. Piccardi, M. Peccianti, and G. Assanto, Phys. Rev. A **75**, 063835 (2007).
[18] A. Minovich, D. N. Neshev, A. S. Desyatnikov, W. Krolikowski, and Y. S. Kivshar, Opt. Express **17**, 23610 (2009).
[19] Y. V. Izdebskaya, A. S. Desyatnikov, and Y. S. Kivshar, Phys. Rev. Lett. **111**, 123902 (2013).
[20] H. Michinel, M. J. Paz-Alonso, and V. M. Pérez-García, Phys. Rev. Lett. **96**, 023903 (2006).
[21] A. Alexandrescu, H. Michinel, and V. M. Pérez-García, Phys. Rev. A **79**, 013833 (2009).
[22] S. K. Adhikari, Phys. Rev. E **94**, 032217 (2016).
[23] As this is an out-of-equilibrium system, an EOS cannot be defined, and the energy per particle is the relevant quantity with which to compare.
[24] M. Valiente and P. Öhberg, Phys. Rev. A **94**, 051606 (2016).
[25] I. Ferrier-Barbut, H. Kadau, M. Schmitt, M. Wenzel, and T. Pfau, Phys. Rev. Lett. **116**, 215301 (2016).
[26] M. Schmitt, M. Wenzel, F. Bttcher, I. Ferrier-Barbut, and T. Pfau, Nature (London) **539**, 259 (2016).
[27] L. Chomaz, S. Baier, D. Petter, M. J. Mark, F. Wächtler, L. Santos, and F. Ferlaino, Phys. Rev. X **6**, 041039 (2016).
[28] C. R. Cabrera, L. Tanzi, J. Sanz, B. Naylor, P. Thomas, P. Cheiney, and L. Tarruell, Science **359**, 301 (2018).
[29] P. Cheiney, C. R. Cabrera, J. Sanz, B. Naylor, L. Tanzi, and L. Tarruell, Phys. Rev. Lett. **120**, 135301 (2018).
[30] A. Couairon and A. Mysyrowicz, Phys. Rep. **441**, 47 (2007).
[31] T. Roger, C. Maitland, K. Wilson, N. Westerberg, D. Vocke, E. M. Wright, and D. Faccio, Nat. Commun. **7**, 13492 (2016).
[32] C. J. Pethick and H. Smith, *Bose Einstein Condensation in Dilute Gases*, 2nd ed. (Cambridge University Press, Cambridge, England, 2008).
[33] D. Vocke, K. Wilson, F. Marino, I. Carusotto, E. M. Wright, T. Roger, B. P. Anderson, P. Öhberg, and D. Faccio, Phys. Rev. A **94**, 013849 (2016).
[34] Note that this ansatz is of a slightly different functional form than the droplet found in Ref. [14]; i.e., it is Gaussian instead of exponential. The difference is, however, small, and the ansatz used here corresponds closely to the experimental input and should be thought of as an initial condition.
[35] See Supplemental Material at http://link.aps.org/supplemental/10.1103/PhysRevLett.121.133903 for details of the spatial evolution corresponding to the photon droplet dynamics shown in Fig. 2.
[36] The only relevant backreflection (of the order of 8%) is from the very first ($P0$) and last ($P4$) facets. The glass slabs are butted together with good optical contact between adjoining slabs, resulting in negligible backreflections from any intermediate interfaces along the propagation direction.
[37] A. Mair, A. Vaziri, G. Weihs, and A. Zeilinger, Nature (London) **412**, 313 (2001).
[38] J. Leach, B. Jack, J. Romero, A. K. Jha, A. M. Yao, S. Franke-Arnold, D. G. Ireland, R. W. Boyd, S. M. Barnett, and M. J. Padgett, Science **329**, 662 (2010).
[39] R. Liu, D. B. Phillips, F. Li, M. D. Williams, D. L. Andrews, and M. J. Padgett, J. Opt. **17**, 045608 (2015).
[40] The experimental error for $\Delta_+ - \Delta_-$ is calculated by taking the standard deviation of the residuals from the fit to each measured amplitude $|A_{\mathrm{HP(LP)},\pm}|^2$ and then summing the errors in quadrature.
[41] L. F. Gomez, K. R. Ferguson, J. P. Cryan, C. Bacellar, R. M. P. Tanyag, C. Jones, S. Schorb, D. Anielski, A. Belkacem, C. Bernando, R. Boll, J. Bozek, S. Carron, G. Chen, T. Delmas, L. Englert, S. W. Epp, B. Erk, L. Foucar, R. Hartmann *et al.*, Science **345**, 906 (2014).
[42] R. J. A. Hill and L. Eaves, Phys. Rev. Lett. **101**, 234501 (2008).